THE JOURNAL OF PHYSICAL CHEMISTRY C

Article

pubs.acs.org/JPCC

In Situ Spectroelectrochemical Investigation of Ge, Si, and Si_xGe_{1-x} Electrodeposition from an Ionic Liquid

Abhishek Lahiri,*[,†] Mark Olschewski,[†] Oliver Höfft,[†] Sherif Zein El Abedin,[†,‡] and Frank Endres*[,†]

[†]Institute of Electrochemistry, Clausthal University of Technology, Arnold-Sommerfeld-Str. 6, 38678 Clausthal-Zellerfeld, Germany

[‡]Electrochemistry and Corrosion Laboratory, National Research Centre, Dokki, Cairo, Egypt

Supporting Information

ABSTRACT: We report on in situ UV−vis spectroscopic measurement during the electrodeposition of silicon, germanium, and silicon−germanium alloys from an ionic liquid. From the spectroscopic analysis, the potential-dependent formation and growth of Ge, Si, and Si_xGe_{1-x} nanoparticles were evaluated. The possible formation of adlayers and an underpotential deposition of Si on Ge during silicon and germanium electrodeposition are also discussed.

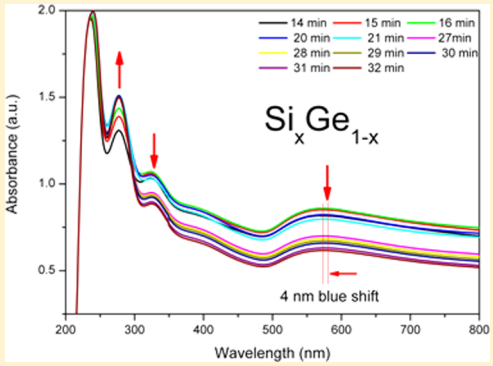

INTRODUCTION

Silicon, germanium, and their compounds are important semiconductors in the fields of electronics and photonics.[1,2] Both germanium and silicon nanoparticles show quantum confinement effects[3] which are manifested by photoluminescence and emission of visible light.[4] The luminescence effect is still not fully understood and has also been related with silicon surface termination.[5] Nevertheless, these phenomena at the nanoscale open up potential applications in the fields of optoelectronics such as in developing light-emitting diodes,[6] biological labeling,[6] and also photovoltaic cells.[7]

Considerable research has been done on the electrodeposition of germanium and silicon in organic solutions.[2] However, the electrochemical window of organic solvents is limited, and the effect of impurities is unclear; thus, the electrodeposition process only leads to the formation of thin layers.[8,9] For example, Huang et al.[8] reported the deposition of germanium films on silicon substrates from 1,3-propanediol wherein the deposit contained impurities such as N and C. Similarly, silicon is obtained as a porous material which was quickly oxidized under air, forming a white layer.[9] In comparison, electrodeposition of these semiconductors in ionic liquids leads to thicker deposits with an insignificant impurity level, which mainly results from ionic liquid adsorption at the surface. Our group has extensively investigated the electrodeposition of silicon and germanium from ionic liquids.[10−12] The electrochemical window of the ionic liquid 1-butyl-1-methylpyrrolidinium bis-(trifluoromethylsulfonyl)amide is wide enough to allow Si deposition from $SiCl_4$.[11] Further evidence on the silicon deposition was obtained using in situ scanning tunneling microscopy (STM) and scanning tunneling spectroscopy (STS)[13] where silicon islands had a band gap of 1.1 ± 0.2 eV. Germanium was electrodeposited from GeX_4 (X = Cl, Br, I) in 1-butyl-3-methylimidazolium hexafluorophosphate ([BMIm]PF_6).[14] It should be mentioned here that ionic liquids containing PF_6^- or BF_4^- are very sensitive to moisture;[15] thus, handling these liquids is quite challenging. However, around the year 2000 these liquids were among the first ones that were investigated in more depth for electrochemistry. Recently, it was shown by quartz crystal microbalance (EQCM) that the deposition of Si from $SiCl_4$ occurs via a four-electron reduction step. The authors also discussed the influence of ionic liquid solvation layers.[16] In situ STM and STS were done to elucidate the Ge electrodeposition process, and from STS measurement a band gap of 0.7 ± 0.1 eV was obtained.[14] In ref 12, it was shown that interesting colors appear during the deposition of Si_xGe_{1-x} from 1-butyl-1-methylpyrrolidinium bis-(trifluoromethylsulfonyl)amide ionic liquid. In order to further investigate the deposition mechanism and to better understand the origin of the observed colors of the deposit, in situ UV−vis spectroelectrochemistry has been performed for this study.

In situ UV−vis spectroelectrochemistry is an important method to assess the reaction mechanism in both liquids and solids. Hitherto, this technique has mainly been used to study redox reactions of organic radicals or of complex formations in inorganic species and metal−organic framework materials.[17,18] Solid-state UV−vis spectroelectrochemistry has been less studied[19,20] and has not yet been applied during electrodeposition processes in ionic liquids. In this paper, we present

Received: September 28, 2012
Revised: December 25, 2012
Published: January 7, 2013

ACS Publications © 2013 American Chemical Society

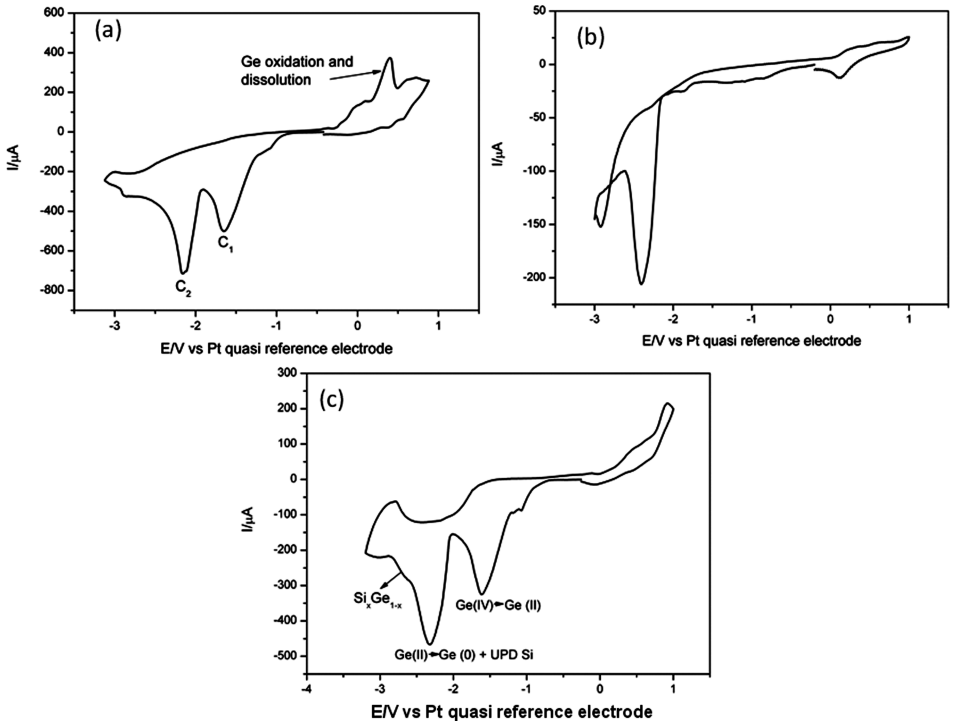

Figure 1. (a) CV of 0.1 M $GeCl_4$, (b) CV of 0.1 M $SiCl_4$, and (c) CV of 0.1 M $SiCl_4$ and 0.1 M $GeCl_4$ in the ionic liquid. 0.1 M $GeCl_4/SiCl_4$ was made by mixing equimolar amounts of 0.1 M $GeCl_4$ and $SiCl_4$ in the ionic liquid. Ionic liquid for all experiments: 1-butyl-1-methylpyrrolidinium bis(trifluoromethylsulfonyl)amide. Substrate: polycrystalline gold. Scan rate: 10 mV/s. Room temperature.

that in situ UV−vis spectroscopy can be employed to study the electrodeposition process of silicon, germanium and Si_xGe_{1-x}.

EXPERIMENTAL SECTION

1-Butyl-1-methylpyrrolidinium bis(trifluoromethylsulfonyl)-amide was purchased in the highest available quality from Io-Li-Tec (Germany) and was used after drying under vacuum at 100 °C to remove the water content to below 2 ppm. This liquid has a sufficiently wide electrochemical window to allow Si deposition; furthermore, its interfacial behavior is relatively well-known. $GeCl_4$ (99.9999%) and $SiCl_4$ (99.999%) were purchased from Alfa Aesar. The working electrode in the experiment was a sputtered film of gold on glass. The Au was cleaned by refluxing it in isopropanol at 90 °C for 2 h. Prior to experiments, the gold was carefully heated in a hydrogen flame to remove any surface contamination. Platinum wires were used as a counter and a quasi reference electrode which gave quite a good stability (±10 mV variation) in the ionic liquid throughout the experiments. The electrochemical cell was made of Teflon and clamped over a Teflon-covered Viton O-ring onto the substrate, yielding a geometric surface area of 0.3 cm^2. Prior to the experiments, the Teflon cell and the O-ring were cleaned in a mixture of 50:50 vol % of concentrated H_2SO_4 and H_2O_2 (35%) followed by refluxing in distilled water.

The electrochemical measurements were performed in an argon-filled glovebox with water and oxygen contents of below 2 ppm (OMNI-LAB from Vacuum Atmospheres) by using a VersaStat II (Princeton Applied Research) potentiostat/galvanostat controlled by powerCV software. The entire scan rate during cyclic voltammetry was 10 mV s^{-1}.

In situ spectroelectrochemical experiments were conducted with a Cary 5000 UV−vis−IR spectrometer. The spectroelctrochemical cell was a quartz cuvette (ALS, Japan) having a path length of 0.5 cm. A gold mesh (ALS, Japan) was used as a working electrode. The quartz cell and the gold mesh were cleaned thoroughly in isopropanol and acetone prior to each experiment. Pt wires were used as both reference and counter electrodes and were cleaned in a hydrogen flame. The cell was assembled inside the Ar-filled glovebox. The setup was then introduced into the UV−vis−NIR device and connected to a Materials M 510 potentiostat/galvanostat. A background UV scan was taken for the electrolyte at open circuit potential and was used to subtract from subsequent measurements. UV−vis spectra were continuously measured for each applied electrode potential at a scan rate of 600 nm min^{-1}.

RESULTS AND DISCUSSION

Figures 1a, 1b, and 1c show cyclic voltammograms (CV) of 0.1 M $GeCl_4$, 0.1 M $SiCl_4$, and 0.1 M $GeCl_4/SiCl_4$, respectively, in the ionic liquid 1-butyl-1-methylpyrrolidinium bis-(trifluoromethylsulfonyl)amide on gold at room temperature. In Figure 1a, two main reduction peaks C1 and C2 are observed which correspond to the reduction of Ge(IV) to Ge(II) and to Ge(II) to Ge(0). In the anodic direction above +0.4 V, oxidation and dissolution of the deposited Ge take place. In comparison, the reduction of silicon shows only one main reduction peak at −2.45 V, corresponding to the four-electron reduction process of Si(IV) to Si. The CV curve in Figure 1c shows two main reduction peaks and two shoulders. The first process around −1 V could be due to the underpotential deposition of germanium on gold and to the formation of Si_xCl_y compounds. The second one at −1.6 V corresponds to the reduction of Ge(IV) to Ge(II). The third process at −2.2 V is due to the reduction of Ge(II) to Ge(0) and possibly due to some underpotential deposition (UPD) of silicon on Ge.

The fourth process at −2.8 V is the formation of Si_xGe_{1-x}. These results are consistent with previously published data.[12] In

dx.doi.org/10.1021/jp309646r | J. Phys. Chem. C 2013, 117, 1722−1727

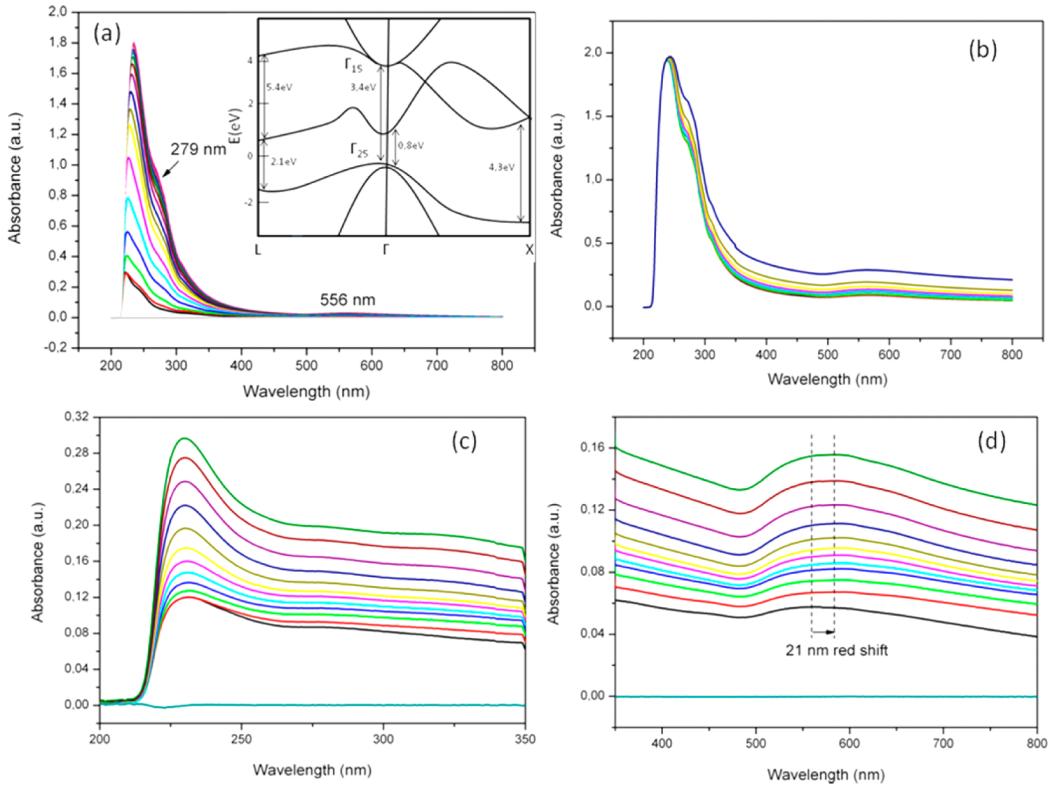

Figure 2. (a) Changes in the absorption spectra on applying the potential for the reduction of Ge(IV) to Ge(II). Each spectrum corresponds to 1 min of electrodeposition. Electrolyte solution: 0.1 M $GeCl_4$ in 1-butyl-1-methylpyrrolidinium bis(trifluoromethylsulfonyl)amide. Inset shows the schematic band structure of Ge (after ref 22). (b) On applying the potential for the reduction of Ge(II) to Ge. (c) Absorption spectra at (200−350 nm) at the potential at −2.3 V for the electrodeposition of germanium. (d) UV−vis spectra during Ge deposition between 350 and 800 nm at −2.3 V.

the anodic regime, a broad reduction peak starting at −2.6 V is observed which also correlates to the deposition of Si_xGe_{1-x} and Ge. Such a phenomenon has been previously observed during the electrodeposition of silicon and was related to a certain passivation by an ionic liquid layer adsorbed on the electrodeposited materials.[13] This layer might be partially decomposed.

In order to understand the electrodeposition process, we performed in situ UV−vis spectroelectrochemistry experiments. Figure 2a shows the UV−vis spectra of 0.1 M $GeCl_4$ in 1-butyl-1-methylpyrrolidinium bis(trifluoromethylsulfonyl)amide at a potential corresponding to C1 (−1.6 V) in Figure 1a as a function of time. The UV−vis spectra were measured between 200 and 800 nm as it was shown in ref 12 that the appearance of optical colors during the formation of Si_xGe_{1-x} must be due to the absorption of light in the range of 380 and 700 nm. With time a prominent rise in the peak at 220 nm is evident. This peak is due to the formation of Ge(II) species in the ionic liquid.[21] After about 10 min at constant potential, a shoulder at 279 nm and a small broad peak at 556 nm are observed. The 279 nm peak is associated with a direct transition at X in the Brillouin zone, and the peak at 556 nm is the transition at L of elemental Ge, according to literature data.[22] The transitions in the Brillouin zone have been depicted in the inset in Figure 2a. These peaks correspond according to ref 23 to the formation of Ge nanoparticles of about 3.5 nm in size.

These peaks grow with time at this electrode potential. Such a formation of Ge nanoparticles could be due to the underpotential deposition (UPD) of germanium on gold which occurs along with the reduction of Ge(IV) to Ge(II) species. Evidence for Ge UPD was shown by in situ STM,[14] and the UV−vis data are mainly consistent with data from the literature. On applying the potential at C2 (−2.3 V, Figure 1a), an increase of the shoulder at 279 nm and of the peak at 556 nm is observed. Furthermore, an overall increase in the absorption peak occurs which can be associated with a Mie scattering effect. With increased deposition time, a red-shift of 4 to 560 nm takes place. The red-shift in the peak is likely due to the increased particle size and the possible aggregation of Ge nanoparticles.[22] Comparing Figure 2b with Figure 2a, no significant difference in the absorption peaks is observed. Furthermore, no Mie scattering is observed in Figure 1a, which further supports that a UPD of Ge occurred at the potential of C1. As UPD is a surface phenomenon, no nanoparticles are formed in the electrolyte, and therefore Mie scattering is not observed.

Figures 2c and 2d show the absorption spectra on directly applying the potential at C2 (−2.3 V). With time, an increase of the absorption peak at 225 nm takes place which corresponds to the formation of Ge(II) species.[21] A shallow and broad peak at 280 nm is observed associated with the transition at X in the Brillouin zone. The overall increase in absorption could be due to Mie scattering. Figure 2d shows the absorption spectra between 350 and 800 nm. It is evident that with time there is an increase in overall absorption and a slight red-shift of 21 nm from 560 to 581 nm. This red-shift is due to an increase in particle size and agglomeration. Furthermore, the results suggest that during initial deposition quantum confinement effects in Ge nanoparticles take place, influencing the absorption peak position. However, this effect was lacking in

dx.doi.org/10.1021/jp309646r | J. Phys. Chem. C 2013, 117, 1722−1727

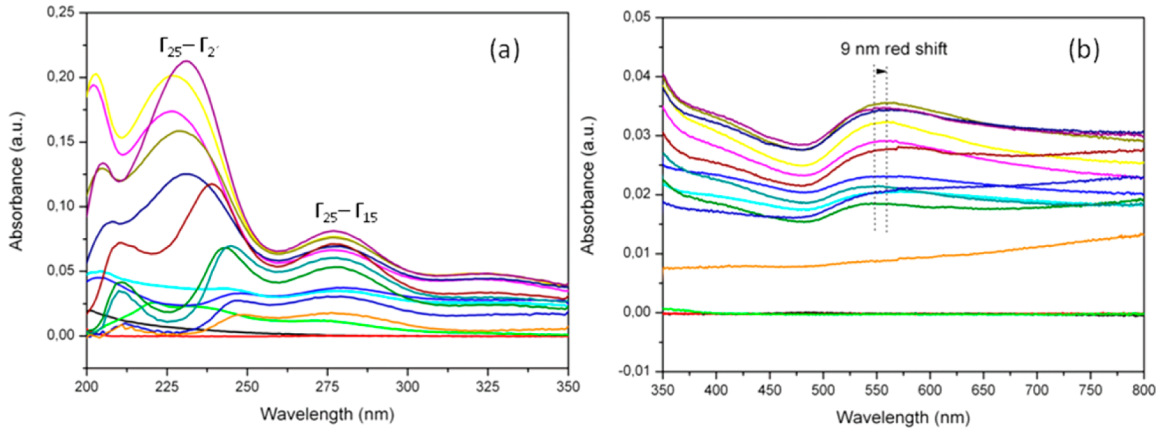

Figure 3. (a) Changes in absorption spectra during the electrodeposition of silicon between 200 and 350 nm and (b) between 350 and 800 nm. Each spectrum corresponds to 1 min of electrodeposition process. Electrolyte solution: 0.1 M $SiCl_4$ in 1-butyl-1-methylpyrrolidinium bis(trifluoromethylsulfonyl)amide.

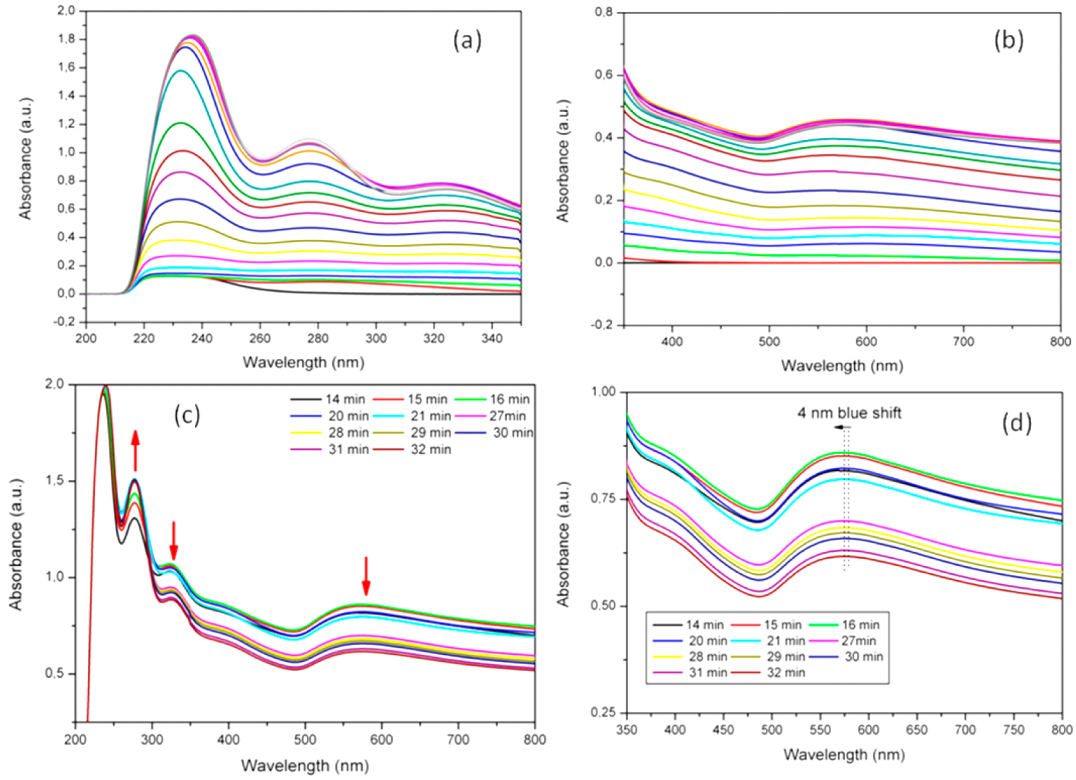

Figure 4. (a) Change in absorption spectrum between 200 and 350 nm on applying a potential of −2.4 V. Each spectrum corresponds to 1 min of electrodeposition process. The red arrows indicate the change in absorbance. Electrolyte solution: 0.1 M $GeCl_4$ + 0.1 M $SiCl_4$ in 1-butyl-1-methylpyrrolidinium bis(trifluoromethylsulfonyl)amide. (b) Between 350 and 800 nm. (c, d) Changes in UV spectra on applying a potential of −2.8 V.

Figure 2b wherein the potential was applied after the formation of Ge(II) species. This indicates that a considerably lower amount of Ge was deposited in the experiment shown in Figure 2b. It was previously reported that the deposition of Ge from $GeCl_2$ is sluggish in 1-butyl-1-methylpyrrolidinium bis-(trifluoromethylsulfonyl)amide,[12] and the same process has likely occurred here (Figure 2b).

Figure 3 shows the absorption spectra during the electrodeposition of silicon at −2.5 V. At the initial stages of the deposition process, no peaks are observed in the UV spectra (curves red and black in Figure 3a). However there is a rise in the absorption peak around 225 nm which could be associated with the adsorption of the organic cation on the electrode surface. Such an adsorption process has been previously reported using in situ STM studies.[13] After 3 min of electrodeposition, the green curve in Figure 3a shows three peaks at 275, 235, and 224 nm. These peaks may be the formation of subspecies (Si_xCl_{2y+2}) of silicon adsorbed on the gold mesh electrode. In situ Raman analysis has shown the possibility for the formation of such subspecies.[24] With increase in time various complex processes take place wherein the peaks at 235 and 275 nm (green curve) separate to form peaks at 245 and 220 nm (orange curve). Finally, the peaks converge to two prominent peaks at 275 and 226 nm. There is no clear trend in

dx.doi.org/10.1021/jp309646r | J. Phys. Chem. C 2013, 117, 1722−1727

the evolving spectra which is at least a strong hint for complex electrochemical processes in the initial stages.

Also, the potential-dependent formation of solvation layers of the ionic liquid on the Au might have contributed to such complicated changes in the absorbance. Such solvation layers have been previously investigated using in situ STM and AFM.[25] From AFM analysis it was found that 1-butyl-1-methylpyrrolidinium bis(trifluoromethylsulfonyl)amide forms multiple solvation layers at the gold interface.[25] Furthermore, an in situ STM analysis showed a type of a restructuring of the Au (111) interface and also formation of wormlike patterns, induced by ionic liquid adsorption.[25] Although in our experiments a polycrystalline mesh Au electrode was used, the formation of solvation layers cannot be neglected. The peak at 275 nm corresponds to the Γ_{25} to Γ_{15} transition at X in the Brillouin zone, and the peak at 226 is the Γ_{25} to $\Gamma_{2'}$ transition.[26] Figure S1 in the Supporting Information shows the energy band structure of silicon near the bandgap. Furthermore, blue- and red-shifts are observed at 226 nm which might be due to formation of different sizes of silicon particles. The overall absorption also increases due to Mie scattering from the silicon nanoparticles. The shallow broad peak at 325 nm might be correlated with the second direct transition at X of the Brillouin zone in silicon clusters.[26] In the wavelength between 350 and 800 nm (Figure 3b), a prominent peak at 550 nm is observed. This peak corresponds to the indirect nature of the band gap.[26] Also, a red-shift of 9 nm is observed which could be due to the increase in nanoparticle size and agglomeration. The red-shifting indicates the possibility of quantum confinement effects at initial stages of silicon deposition.

In order to evaluate the formation of Si_xGe_{1-x}, the initial potential was held close to that one of Ge bulk deposition. Figure 4a shows the changes in absorption spectra between 200 and 350 nm. In the beginning, only one peak at 225 nm is observed which is due to the formation of the Ge(II) species. With further increase in electrodeposition time, a red-shift to 235 nm is evident which could be due to the formation of silicon nanoparticles along with Ge. Additionally, a peak at 325 nm is also observed which relates well with the transition at X of the Brillouin zone due to the formation of silicon clusters.[26] Consequently, there is a strong evidence that a UPD of Si occurs during the bulk deposition of germanium. Figure 4b shows the type of an evolving shallow peak at 570 nm, which could be due to the direct transition at L in Ge nanoparticles as a relatively sharp peak forms in this region for silicon nanoparticles. The shallow peak also indicates a large size distribution of nanoparticles. From the present measurements we cannot decide without doubt to which extent this broad peak is due to Ge and to Si. Figure 4c shows the absorption spectra after 14 min during the deposition of Si_xGe_{1-x} at a potential of −2.8 V where Si_xGe_{1-x} deposition has to be expected.

Figure S2 shows the total change in absorption spectra during the electrodeposition. Three prominent peaks at 275, 325, and 580 nm could be observed whose absorbance grew with time (Figure 4c). After 16 min of deposition, the absorbance peaks at 580 nm (Figure 4d) and 325 nm started to decrease whereas the peak at 275 nm continued to increase. Furthermore, the peak at 580 nm is blue-shifted by 4 nm (Figure 4d). Botti et al.[27] showed using density functional theory (DFT) calculation that a quantum confinement effect, and the inclusion of Si in the Ge matrix leads to the blue-shifting and to the reduction of the absorption peak around 540 nm in their study. Similar phenomenon is observed, although here at 580 nm (Figure 4d), the shifting and decrease in absorption can be associated with the formation of Si_xGe_{1-x} and with a quantum confinement effect.[27] The 40 nm discrepancy between calculations in the absorption spectra and experimental results is difficult to explain at present and might need further studies. The decrease in the 325 nm peak could be associated with a decrease in silicon cluster formation due to alloying. Similar spectra could also be observed at other potentials of −2.9 and −2.7 V which are also associated with the formation of Si_xGe_{1-x}. Therefore, from the UV absorbance spectra in Figures 4c and 4d, we can conclude that initially there is codeposition of Si and Ge nanoparticles which then combine together to form Si_xGe_{1-x}.

CONCLUSION

The electrodeposition of germanium, silicon, and Si_xGe_{1-x} alloy has been investigated using in situ UV−vis spectroelectrochemistry. From the spectroscopic analysis the underpotential deposition of Ge on gold at the Ge(IV) to Ge(II) reduction process has been demonstrated. A red-shift at higher wavelengths during the deposition of bulk germanium has been observed which could be related to the formation of clusters. A similar effect is also observed in the case of silicon, although the deposition phenomenon is much more complex. During the formation of Si_xGe_{1-x} alloy, it appears that silicon and germanium are initially codeposited after which the formation of silicon−germanium alloy starts.

ASSOCIATED CONTENT

Supporting Information

A schematic band diagram of silicon (Figure S1); complete changes in the in situ UV−vis spectra during the formation of Si_xGe_{1-x} alloy (Figure S2). This material is available free of charge via the Internet at http://pubs.acs.org.

AUTHOR INFORMATION

Corresponding Author

*E-mail: abhishek.lahiri@tu-clausthal.de (A.L.); frank.endres@tu-clausthal.de (F.E.).

Notes

The authors declare no competing financial interest.

ACKNOWLEDGMENTS

Financial support by the BMBF project HELION and by the Lower Saxony graduate school GEENI is gratefully acknowledged.

REFERENCES

(1) Lehmann, V. *Electrochemistry of Silicon: Instrumentation, Science, Materials and Applications*; Wiley-VCH: Weinheim, 2002.

(2) Zein El Abedin, S.; Endres, F. Electrodeposition of metals and semiconductors in air- and water-stable ionic liquids. *ChemPhysChem* **2006**, *7* (1), 58−61.

(3) Konchenko, A.; Nakayama, Y.; Matsuda, I.; Hasegawa, S.; Nakamura, Y.; Ichikawa, M. Quantum confinement observed in Ge nanodots on an oxidized Si surface. *Phys. Rev. B* **2006**, *73* (11), 113311−113314.

(4) Zacharias, M.; Fauchet, P. M. Blue luminescence in films containing Ge and GeO_2 nanocrystals: The role of defects. *Appl. Phys. Lett.* **1997**, *71* (3), 380−382.

(5) Sa'ar, A. On the origin of photoluminescence from silicon nanostructures: a new perspective. *Phys. Status Solidi C* **2011**, *8* (6), 1764−1768.
(6) Alivisatos, P. The use of nanocrystals in biological detection. *Nat. Biotechnol.* **2004**, *22* (1), 47−52.
(7) Hochbaum, A. I.; Yang, P. Semiconductors nanowires for energy conversion. *Chem. Rev.* **2010**, *110* (1), 527−546.
(8) Huang, Q.; Bedell, S. W.; Saenger, K. L.; Copel, M.; Deligianni, H.; Romankiw, L. T. Single-crystalline germanium thin films by electrodeposition and solid-phase epitaxy. *Electrochem. Solid-State Lett.* **2007**, *10* (11), D124−D126.
(9) Nishimura, Y.; Fukunaka, Y. Electrochemical reduction of silicon tetrachloride in non-aqueous solvents. *Electrochim. Acta* **2007**, *53* (1), 111−116.
(10) Endres, F. Electrodeposition of a thin germanium film on gold from a room temperature ionic liquid. *Phys. Chem. Chem. Phys.* **2001**, *3* (15), 3165−3174.
(11) Zein El Abedin, S.; Borissenko, N.; Endres, F. Electrodeposition of nanoscale silicon in a room temperature ionic liquid. *Electrochem. Commun.* **2004**, *6* (5), 510−514.
(12) Al-Salman, R.; Zein El Abedin, S.; Endres, F. Electrodeposition of Ge, Si and Si_xGe_{1-x} from an air- and water-stable ionic liquid. *Phys. Chem. Chem. Phys.* **2008**, *10* (31), 4650−4657.
(13) Borisenko, N.; Zein El Abedin, S.; Endres, F. In situ STM investigation of gold restructuring and of silicon electrodeposition on Au (111) in the room temperature ionic liquid 1-butyl-1-methylpyrrolidinium Bis(trifluoromethylsulfonyl)imide. *J. Phys. Chem. B* **2006**, *110* (12), 6250−6256.
(14) Endres, F.; Zein El Abedin, S. Nanoscale electrodeposition of germanium on Au (111) from an ionic liquid: an in situ STM study of phase formation. *Phys. Chem. Chem. Phys.* **2002**, *4* (9), 1640−1648.
(15) Freire, M. G.; Neves, C. M. S. S.; Marrucho, I. M.; Coutinho, J. A. P.; Fernandes, A. M. Hydrolysis of tetraflouoroborate and hexaflouorophosphate counter ions in imazolium-based ionic liquids. *J. Phys. Chem. A* **2010**, *114* (11), 3744−3749.
(16) Komadina, J.; Akiyoshi, T.; Ishibashi, Y.; Fukunaka, Y.; Homma, T. Electrochemical quartz crystal microbalance study of Si electrodeposition in ionic liquid. *Electrochim. Acta* **2012**, DOI: 10.1016/j.electacta.2012.07.043.
(17) Kaim, W.; Fiedler, J. Spectroelectrochemistry: the best of two worlds. *Chem. Soc. Rev* **2009**, *38* (12), 3373−3382.
(18) Dunsch, L. Recent advances in in situ multi-spectroelectrochemistry. *J. Solid State Electrochem.* **2011**, *15* (7), 1631−1646.
(19) Barbante, G.; Hogan, C.; Hughes, A. Solid state spectroelectrochemistry of microparticles of ruthenium diimine complexes immobilised on optically transparent electrode. *J. Solid State Electrochem.* **2009**, *13* (4), 599−608.
(20) Bonifas, A. P.; McCreery, R. L. Solid state spectroelectrochemistry of redox reactions of polypyrrole/oxide molecular heterojunctions. *Anal. Chem.* **2012**, *84* (5), 2459−2465.
(21) Nikol, H.; Becht, A.; Vogler, A. Photoluminescence in germanium (II), tin (II) and lead (II) chloride complexes in solution. *Inorg. Chem.* **1992**, *31* (15), 3277−3279.
(22) Wilcoxon, J. P.; Provencio, P. P.; Samara, G. A. Synthesis and optical properties of colloidal germanium nanocrystals. *Phys. Rev. B* **2001**, *64* (3), 035417−035425.
(23) Hayashi, S.; Fujii, M.; Yamamoto, K. Quantum size effects in Ge microcrystals embedded in SiO_2 thin films. *Jpn. J. Appl. Phys* **1989**, *28*, L1464−L1466.
(24) Nishimura, Y.; Fukunaka, Y.; Miranda, C. R.; Nishida, T.; Nohira, T.; Hagiwara, R. In situ Raman spectroscopy studies of the electrolyte-substrate interface during electrodeposition of silicon in a room-temperature ionic liquid. *ECS Trans.* **2009**, *16* (24), 1−6.
(25) Atkin, R.; Zein El Abedin, S.; Hayes, R.; Gasparotto, L. H. S.; Borisenko, N.; Endres, F. AFM and STM studies on the surface interaction of [BMP]TFSA and [Emim]TFSA ionic liquids with Au (111). *J. Phys. Chem. C* **2009**, *113* (30), 13266−13272.
(26) Wilcoxon, J. P.; Samara, G. A.; Provencio, P. N. Optical and electronic properties of Si nanoclusters synthesized in inverse micelles. *Phys. Rev. B* **1999**, *60* (4), 2704−2714.
(27) Botti, S.; Weissker, H.-C.; Marques, M. A. L. Alloying effects on the optical properties of $Ge_{1-x}Si_x$ nanocrystals from time-dependent density functional theory and comparison with effective-medium theory. *Phys. Rev. B* **2009**, *79* (15), 155440−155446.